Evolutionary Systematics. 8 2024, 183–197 | DOI 10.3897/evolsyst.8.124557

A new species of yellow acorn ant discovered in Italy via integrative taxonomy (*Temnothorax luteus*-complex, Formicidae)

Sándor Csősz[1,2*], Enrico Schifani[3*], Bernhard Seifert[4], Antonio Alicata[5], Matthew M. Prebus[6,7,8]

1 *HUN-REN-ELTE-MTM Integrative Ecology Research Group, Pázmány Péter ave 1/C, Budapest 1117, Hungary*
2 *Department of Systematic Zoology and Ecology, Institute of Biology, ELTE-Eötvös Loránd University, Pázmány Péter ave 1/C, Budapest 1117, Hungary*
3 *Department of Chemistry, Life Sciences and Environmental Sustainability, University of Parma, Parco Area delle Scienze 11/A, 43124 Parma, Italy*
4 *Department of Entomology, Senckenberg Museum für Naturkunde, Am Museum 1, D- 02826 Görlitz, Germany*
5 *Department of Biological, Geological and Environmental Sciences, University of Catania, Via Androne 81, 95124 Catania, Italy*
6 *Social Insect Research Group, School of Life Sciences, Arizona State University, 550 E Orange St., Tempe, AZ 85281, USA*
7 *Department of Integrative Taxonomy of Insects, Institute of Biology, University of Hohenheim, Garbenstraße 30, 70599, Stuttgart, Germany*
8 *KomBioTa – Center for Biodiversity and Integrative Taxonomy Research, University of Hohenheim and State Museum of Natural History Stuttgart, Stuttgart, Germany*

https://zoobank.org/08B37BDD-0B3C-4FEC-A8F8-84DF43A35916

Corresponding author: Sándor Csősz (sandorcsosz2@gmail.com)

Academic editor: Dagmara Żyła ♦ **Received** 2 April 2024 ♦ **Accepted** 17 July 2024 ♦ **Published** 28 August 2024

Abstract

The Mediterranean, a global hotspot for rare ant species, hosts a significant representation of the global diversity of the mainly Holarctic ant genus *Temnothorax*. However, several groups still require significant taxonomic efforts. The taxonomy of the *T. luteus* complex species was revised in 2014 when morphometrics allowed distinguishing two valid species and two synonyms out of four taxa that had been originally described from France. The two species recognized since then are *T. luteus*, distributed from Iberia to the Alps, and the largely sympatric but much more xerothermophilic *T. racovitzai*. In Italy, only a few records of the complex were ever published, and the identity of the Italian population was never thoroughly assessed. We combined morphometrics with phylogenomic data to assess the identity of the *T. luteus* populations that spanned from Sicily to the Italian Alps and discovered that all Italian samples belong to a new cryptic species, which we describe as *T. apenninicus* **sp. nov.** whose glacial refugium was probably in the southern Apennines.

Key Words

Morphometry, genomics, Myrmicinae, Apennines, Sicily, glacial refugium

Introduction

The ant genus *Temnothorax* Mayr, 1861 (Formicidae, Myrmicinae) is mainly distributed across the Holarctic region and northern Neotropics (with a minor presence in the northern Afrotropics) and currently counts about 465 extant species (Prebus 2015, 2017; Bolton 2024). *Temnothorax* ants are generally characterized by small-sized workers and small colonies that often nest inside microspaces such as acorns, rock crevices, empty gastropod shells, or galls (thus earning the name of acorn ants) (Prebus 2017; Seifert 2018; Giannetti et al. 2022a, 2022b). While easily overlooked during field surveys, these ants may play an essential ecological role by preying upon a range of small arthropods (Seifert 2018; Giannetti et al. 2022a, 2022c).

* These authors contributed equally to this work.

Copyright: This is an open access article distributed under the terms of the CC0 Public Domain Dedication.

The description of new *Temnothorax* species has sped significantly during the last few decades (Bolton 2024), while a global phylogenomic framework is now available (Prebus 2017). The Mediterranean region, which is a global hotspot for rare ants (Kass et al. 2022), harbors a high number of narrowly distributed species of *Temnothorax*, whose biogeographic patterns often mirror the intricate paleogeographic and climatic history of the region (Schifani et al. 2022; Wang et al. 2023).

The *Temnothorax luteus* complex of yellowish ground-nesting species has been revised by Seifert et al. (2014), who, using morphometric data, demonstrated it to comprise two separate cryptic species in the western Mediterranean, namely *T. luteus* (Forel, 1897) and *T. racovitzai* (Bondroit, 1918), originally described from France alongside with their synonyms. *T. luteus* was demonstrated to be a senior synonym of *T. tristis* (Bondroit, 1918), and *T. racovitzai* a senior synonym of *T. massiliensis* (Bondroit, 1918), as the previous criteria used to delimit and identify the four taxa proved to be inconsistent (Seifert et al. 2014). The *T. luteus* complex belongs to the *rottenbergii* clade alongside the *T. exilis* and *T. rottenbergii* groups (Schifani et al. 2022). *Temnothorax luteus* and *T. racovitzai* have partly overlapping distributions but are characterized by different ecological preferences: *T. racovitzai* occurs in coastal, xerothermic and relatively open habitats of France and Iberia, which is widespread and common. On the other hand, *T. luteus* ranges from the Iberian Peninsula to the Alps, north to at least 46.6, prefers overall colder sites and higher elevation, and in Iberia, its distribution is more limited (Seifert et al. 2014; Seifert 2018; Arcos and García 2023). Seifert et al. (2014) hypothesized that the two species evolved in two different glacial refugia, namely the Italian peninsula (*T. luteus*) and the Iberian peninsula (*T. racovitzai*), which host significantly different ant faunas and acted as separate glacial refugia (Schifani 2022; Arcos and García 2023; Wang et al. 2023). However, at that time, no samples from Italy, where the complex has rarely been recorded (Baroni Urbani 1971), were available for investigation (Seifert et al. 2014).

We investigated the populations of the *T. luteus* group occurring in Italy by integrating the morphological and phylogenetic data.

Materials and methods

Morphometry

Material examined

This study analyzes the morphometric data of 221 worker individuals belonging to 82 nest samples. Forty worker individuals belonging to 18 nest samples were measured by SC, extending the morphometric dataset of *Temnothorax luteus* complex species published by Seifert et al. 2014 following the same morphometric protocol. In addition, SC measured eight individuals of 3 nest samples that were measured by BS in 2014 to test the reproducibility of the morphometric measurements of the two gaugers (Csősz et al. 2021). The complete list of examined material is listed in Suppl. material 1, including locality information, number of measured individuals.

Protocol for morphometric character recording

All measurements were made with a cross-scale graticule at µm precision using a pin-holding stage, permitting rotations around X, Y, and Z axes with an Olympus SZX16 stereomicroscope with a 1.6× Plan Apochromat objective at a magnification of ×192 for each character by SC. Definitions of morphometric characters are listed in Table 1. Raw data in millimeters are given in Suppl. material 2. We used intraclass correlation coefficients (ICC) to calculate the reproducibility parameter between the dataset measured by BS and the extension added anew by SC via package ICC (Wolak et al. 2012) in R (see Table 1).

Statistical framework on morphometric data—hypothesis formation and testing

We use the toolkit of exploratory data analysis of continuous morphometric data (Seifert et al. 2014; Csősz and Fisher 2016) followed by confirmatory data analysis.

Exploratory analyses via NC-PART clustering

The prior species hypothesis was generated based on workers via Nest Centroid clustering (NC clustering; Seifert et al. 2014) in combination with partitioning algorithms PART (Nilsen and Lingjaerde 2013; Csősz and Fisher 2016) for estimating the number of biologically meaningful clusters. The protocol of this combination was published by Csősz and Fisher (2016), which is now applied with the following specific setups: bootstrap iterations in PART were set to 'b=1000', and the minimum size of clusters was set to 'minSize=5' for both 'hclust' and 'kmeans'. Data input for this analysis was performed as absolute measurements (raw data).

Confirmatory data analyses

The validity of the prior species hypothesis imposed by the exploratory processes was tested via a cross-validated linear discriminant analysis (CV-LDA) using the package MASS (Venables and Ripley 2002). Statistical analyses have been done in R (R Core Team 2023). Conventional LDA and backward stepwise methods were used to create an easy-to-use numeric key for separating species *via* character reduction. Data input for this analysis was performed as absolute measurements (raw data).

Table 1. Abbreviations for morphometric characters, character definitions, and the Intraclass Correlation Coefficient as a reproducibility parameter are presented in different columns.

Abbr.	Definition	ICC (R)
CL	The maximum cephalic length in the median line; the head must be carefully tilted to the position with the true maximum. Excavations of occiput and/or clypeus reduce CL.	0.807
CS	Cephalic size, the arithmetic mean of CL and CW, is a less variable indicator of body size.	NA
CW	The maximum cephalic width is measured across and including the eyes, exceptionally posteriorly of the eyes.	0.966
EYE	Eye-size index: the arithmetic mean of the large (EL) and small diameter (EW) of the elliptic compound eye is divided by CS, i.e. EYE=(EL+EW)/(CL+CW). All structurally visible ommatidia are considered.	0.896
FRS	The distance of the frontal carinae immediately caudal of the posterior intersection points between the frontal carinae and the lamellae dorsal of the torulus. If these dorsal lamellae do not laterally surpass the frontal carinae, the deepest point of scape corner pits may be taken as a reference line. These pits take up the inner corner of the scape base when the scape is entirely switched caudad and produce a dark triangular shadow in the lateral frontal lobes immediately posterior to the dorsal lamellae of the scape joint capsule.	0.983
MW	The maximum mesosoma width; pronotal width in workers.	0.877
ML	The mesosoma length. Measured from the caudal-most point of the propodeal lobe to the transition point between the anterior pronotal slope and anterior propodeal shield (preferentially measured in lateral view; if the transition point is not well defined, use dorsal view and take the center of the dark-shaded borderline between pronotal slope and pronotal shield as an anterior reference point).	0.982
PEH	The maximum petiole height. The straight section of the ventral petiolar profile at node level is the reference line perpendicular to which the maximum height of the petiole node is measured.	0.852
PEL	Diagonal petiolar length in lateral view; measured from the anterior corner of the subpetiolar process to the dorsocaudal corner of the caudal cylinder.	0.931
PEW	maximum width of petiole.	0.988
PoOc	The postocular distance. Use a cross-scaled ocular micrometer and adjust the head to the measuring position of CL. Caudal measuring point: median occipital margin; frontal measuring point: median head at the level of the posterior eye margin. Note that many heads are asymmetric and average the left and right postocular distance.	0.918
PPW	The maximum width of the postpetiole.	0.984
SL	The maximum straight line scape length excluding the articular condyle as the arithmetic mean of both scapes.	0.902
SPBA	The smallest distance of the lateral margins of the spines at their base. This should be measured in the dorsofrontal view since the wider parts of the ventral propodeum do not interfere with the measurement in this position. If the lateral margins of spines diverge continuously from the tip to the base, the smallest distance at the base is not defined. In this case, SPBA is measured at the level of the bottom of the interspinal meniscus.	0.966
SPST	Distance between the center of propodeal stigma and spine tip. The stigma center refers to the midpoint defined by the outer cuticular ring but not to the center of the real stigma opening which may be positioned eccentrically.	0.641
SPTI	The distance of spine tips in dorsal view; if spine tips are rounded or thick, the centers of spine tips are taken as reference points.	0.997

Molecular genetics

Taxon sampling

We gathered three specimens of the new species from two localities and incorporated these with three sequences from a previously published study (Schifani et al. 2022; see Suppl. material 3 for collection data).

Molecular data generation

To generate the genetic data, we extracted DNA, prepared genomic libraries, and performed targeted enrichment of ultraconserved elements (UCEs). We extracted DNA non-destructively from adult worker ants by using a flame-sterilized size 2 stainless steel insect pin to pierce the cuticle of the head, mesosoma, and gaster on the right side of the specimens, then used a DNeasy Blood and Tissue Kit (Qiagen, Inc., Hilden, Germany) following the manufacturer's protocols. We verified DNA extract concentration using a Qubit 3.0 Fluorometer (Invitrogen, Waltham, MA, U.S.A.). We input up to 50 ng of DNA, sheared to a target fragment size of 400–600 bp with a QSonica Q800R sonicator (Qsonica, Newtown, CT, U.S.A.), into a genomic DNA library preparation protocol (KAPA HyperPrep Kit, KAPA Biosystems, Wilmington, MA, U.S.A.). For targeted enrichment of UCEs, we followed the protocol of Faircloth et al. (2015) as modified by Branstetter et al. (2017) using a unique combination of iTru barcoding adapters (Glenn et al. 2019; BadDNA, Athens, GA, U.S.A.) for each sample. We performed enrichments on pooled, barcoded libraries using the catalog version of the Hym 2.5Kv2A ant-specific RNA probes (Branstetter et al. 2017; Arbor Biosciences, Ann Arbor, MI, U.S.A.), which targets 2,524 UCE loci in the Formicidae. We followed the library enrichment procedures for the probe kit, using custom adapter blockers instead of the standard blockers (Glenn et al. 2019; BadDNA, Athens, GA, U.S.A.), and left enriched DNA bound to the streptavidin beads during PCR, as described in Faircloth et al. (2015). Following post-enrichment PCR, we purified the resulting pools using SpeedBead magnetic carboxylate beads (Rohland and Reich 2012; Sigma-Aldrich, St. Louis, MO, U.S.A.) and adjusted their volume to 22 µL. We verified enrichment success and measured size-adjusted DNA concentrations of each pool with qPCR using a SYBR-FASTqPCR kit (Kapa Biosystems, Wilmington, MA, U.S.A.) and a Bio-Rad CFX96 RT-PCR thermal cycler (Bio-Rad Laboratories, Hercules, CA, U.S.A.), subse-

quently combining all pools into an equimolar final pool. We sequenced the final pool in one lane at Novogene (Sacramento, CA, U.S.A.) on Illumina HiSeq 150 cycle Paired-End Sequencing v4 runs (llumina, San Diego, CA, U.S.A.), along with other enriched libraries for unrelated projects.

Dataset construction

We followed the standard PHYLUCE protocol for processing UCEs in preparation for phylogenomic analysis (Faircloth 2016), aligning the monolithic unaligned FASTA file with the phyluce_align_seqcap_align command, using MAFFT (Katoh and Standley 2013) as the aligner (--aligner mafft) and opting not to edge-trim the alignment (–no-trim). We trimmed the resulting alignments with the phyluce_align_get_gblocks_trimmed_alignments_from_untrimmed command in PHYLUCE, which uses GBlocks ver. 0.91b (Castresana 2000), using the following settings: b1 0.5, b2 0.5, b3 12, b4 7. After removing UCE locus information from taxon labels using the command phyluce_align_remove_locus_name_from_nexus_lines, we examined the alignment statistics using the command phyluce_align_get_align_summary_data and generated a dataset in which each locus contains a minimum of 85% of all taxa using the command phyluce_align_get_only_loci_with_min_taxa.

Phylogenetic inference

Because the assumption that the evolutionary rates of sequence data are homogenous is often violated in empirical data (Buckley et al. 2001), we partitioned our UCE loci into sets of similarly evolving sites. To achieve this, we used the command phyluce_align_format_nexus_files_for_raxml which concatenates loci into a single alignment and generates a partition file for input into the SWSC-EN method (Tagliacollo and Lanfear 2018). We used the resulting datablocks as input for partitioning in IQTREE ver. 2.1.2 (Minh et al. 2020), using the command -m MFP+MERGE. Because the combination of gamma and proportion of invariable sites (+I+G) has been demonstrated to result in anomalies in likelihood estimation (Sullivan & Swofford, 2001; Yang, 2006), we set the rate heterogeneity models to a subset that includes everything except the combination of gamma and proportion of invariable sites (-mrate E, I, G) and set the search algorithm to -rclusterf 10. We used the resulting partitioned dataset as input for maximum likelihood tree inference in IQTREE, using 1000 ultrafast bootstrap replicates (-B 1000).

Results

Morphometry

The two clustering methods ‘hclust’ and ‘kmeans’ of PART in combination with NC-clustering resulted in three clusters confirming the validity of the two formerly recognized West European *Temnothorax luteus* complex species *T. luteus* and *T. racovitzai* and a third, Italian cluster took shape. The partitioning methods returned two alternative classifications for two samples, and five more samples have been assigned to outliers out of the total 82 (Fig. 1).

These samples with conflicting identifications were set to wild cards in the first run of confirmatory LDA (Seifert et al. 2014). In the second LDA run and the LOOCV-LDA,

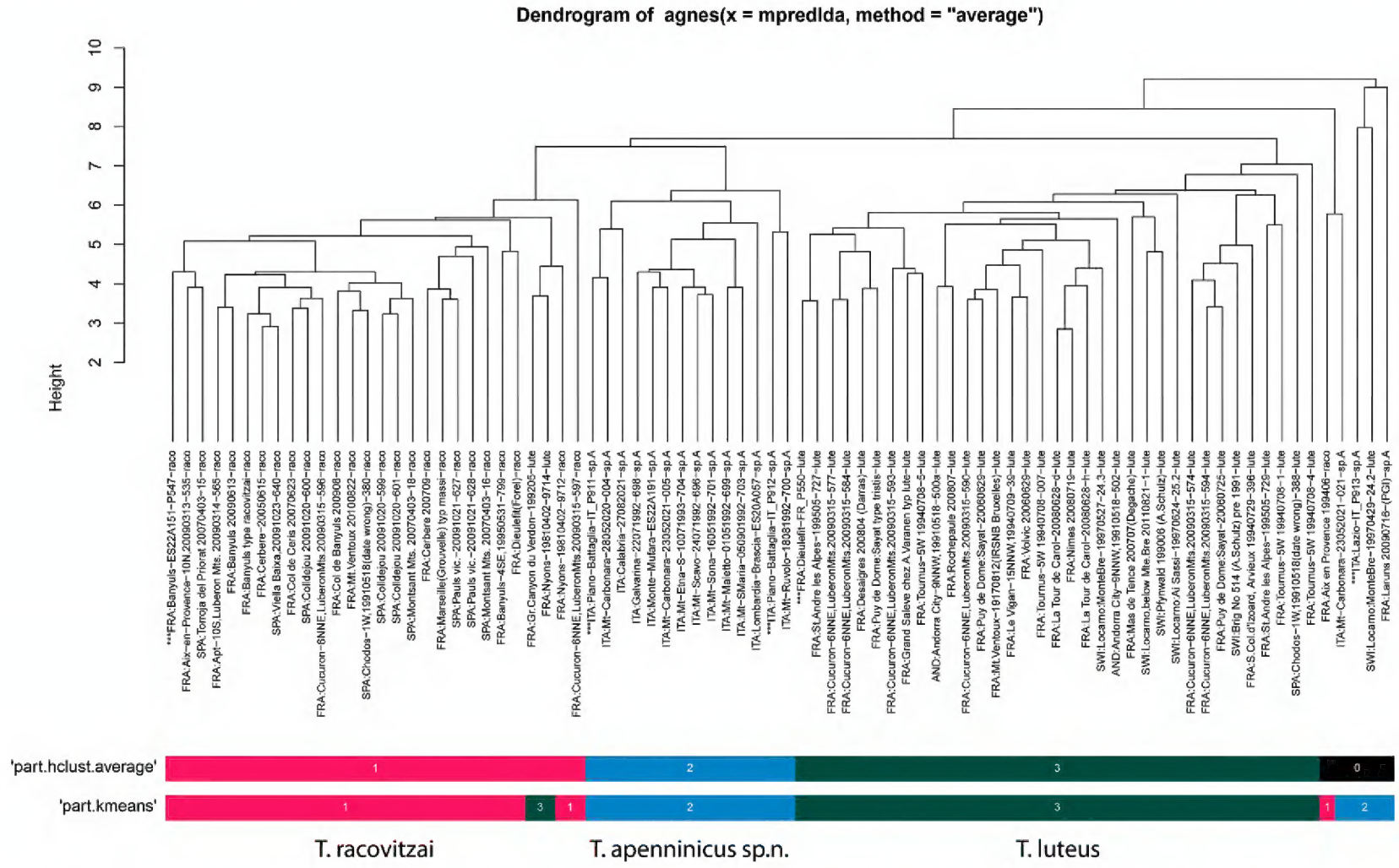

Figure 1. NC-clustering generated cluster solution for *Temnothorax luteus* complex species. *Temnothorax apenninicus* (blue), *T. luteus* (dark green), *T. racovitzai* (purple), and labels represent centroids of nest samples.

these samples are labeled according to the posterior probability values the first LDA returned. The LDA yielded an overall accuracy of 0.97 [95% CI: (0.94, 0.99)] in the classification hypothesis in individuals (Fig. 2) and returned 100% accuracy in the nest sample mean level (Fig. 3).

The cross-validation LDA involving all characters confirmed this classification on an individual level with 95.5% probability (overall accuracy: 0.9545, and 95% CI: 0.918, 0.978) (see Table 2). This means a 4.5% error rate (10 misclassifications out of the 220 individuals) in classification.

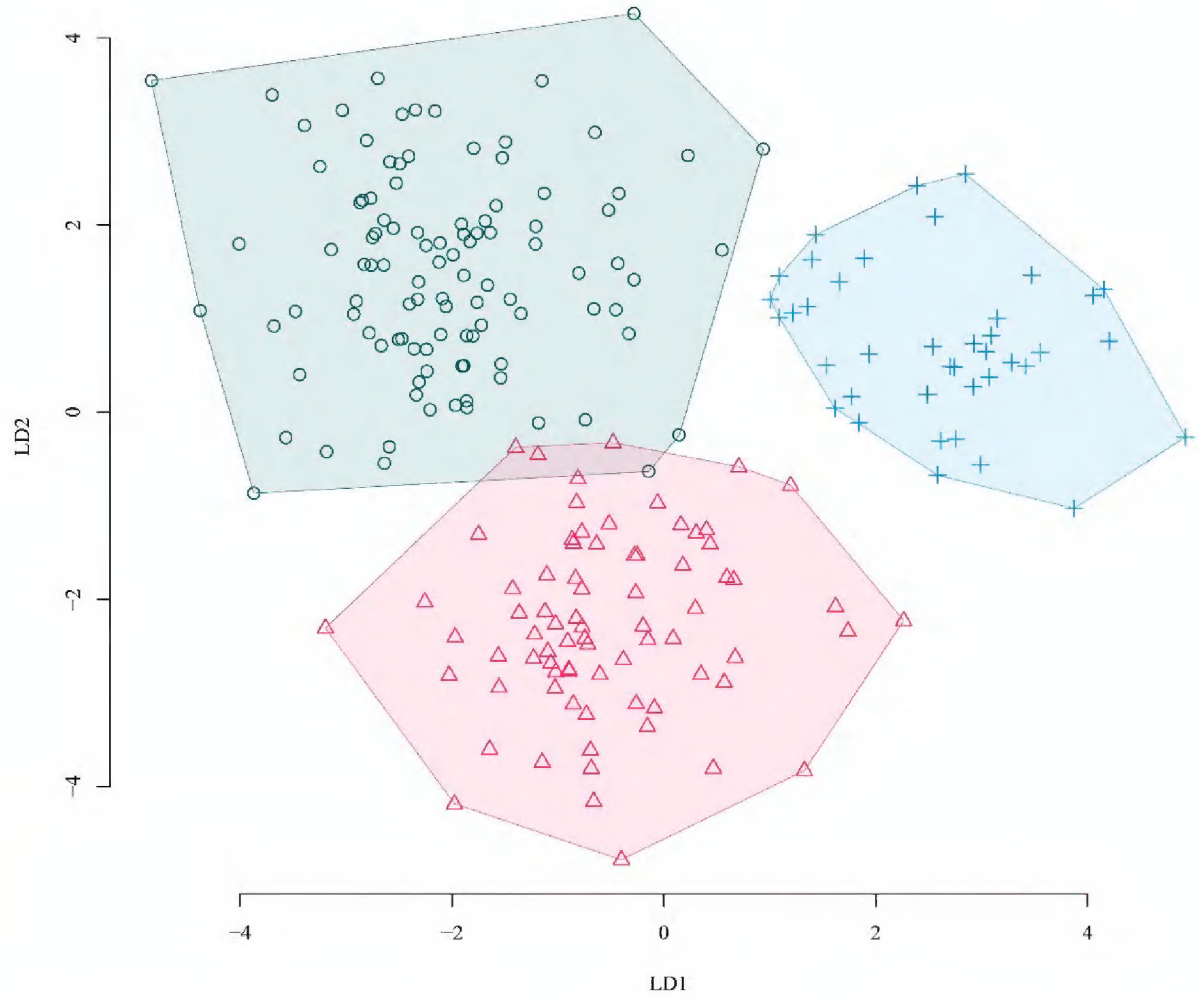

Figure 2. Linear Discriminant Analysis (LDA) plot on worker individuals of *Temnothorax luteus* complex species. The position of *Temnothorax apenninicus* (blue), *T. luteus* (dark green), *T. racovitzai* (purple) individual workers are illustrated in a morphospace defined by LD1 and LD2 scores.

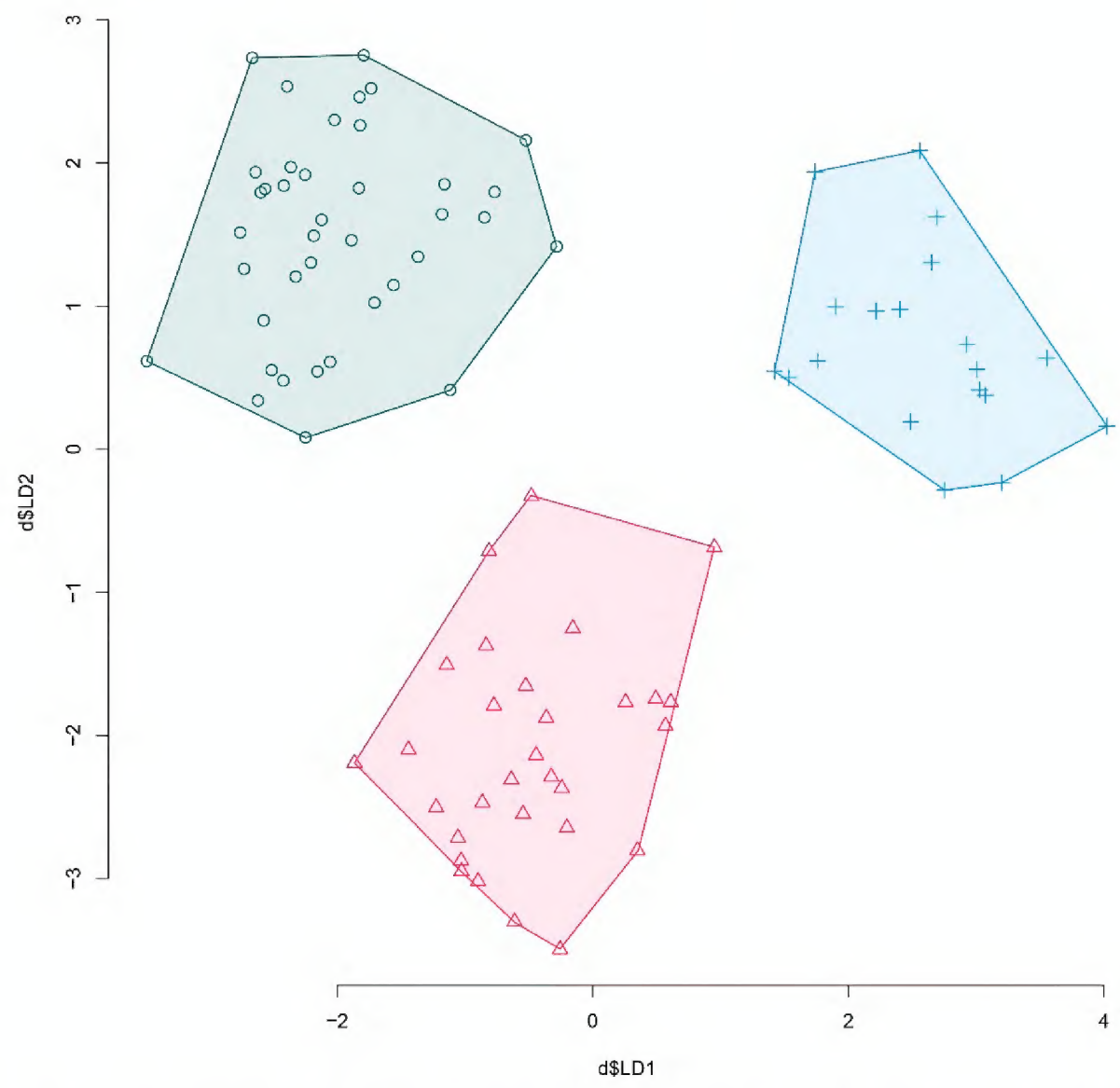

Figure 3. Linear Discriminant Analysis (LDA) plot on nest sample means of *Temnothorax luteus* complex species. The position of *Temnothorax apenninicus* (blue), *T. luteus* (dark green), *T. racovitzai* (purple) nest samples are illustrated in a morphospace defined by LD1 and LD2 scores.

Table 2. Cross-validation table for *Temnothorax apenninicus*, *T. luteus*, and *T. racovitzai* individuals involving 15 morphometric traits.

	T. apenninicus	*T. luteus*	*T. racovitzai*
T. apenninicus	40	3	1
T. luteus	0	98	3
T. racovitzai	0	3	72

Molecular phylogeny

Molecular data processing

Following assembly and UCE extraction, the mean number of loci per sample was 2365, with a mean contig length of 1279 bases and a mean coverage depth of 46.9× (see Suppl. material 4 for summary statistics). Following alignment, trimming, and filtering the full UCE dataset to loci with ≥80% taxon presence (including samples from previous studies), the final dataset had 2385 loci, with a mean locus alignment length of 1118 bases. The concatenated matrix was 2.7 Mb in length, in which 118 Kb were variable, 12 Kb were parsimony informative, with 13.9% missing data. Raw sequence reads newly generated for this study can be found on the NCBI Sequence Read Archive (BioProject PRJNA1092267).

Phylogenetic inference

The partitioning analysis of the dataset in IQTREE resulted in a 118-partition scheme. Model selection resulted in the assignment of 31 unique substitution models. The resulting tree received full statistical support for each node, with the new *Temnothorax* species forming a clade separate from *T. luteus* and *T. racovitzai*, which were recovered as sister species (see Fig. 4).

Temnothorax apenninicus Csősz, Schifani, Seifert, Alicata & Prebus, sp. nov.

https://zoobank.org/40994CF2-689F-4BD5-8F61-155EB5D98E7E

Description. Worker (Fig. 5 A–C, Table 3).

Body color yellow; light brown. Body color pattern concolorous except for the posterior margin of the first gastral tergite which is often characterized by a weak transversal band interrupted in its central portion. Appendages yellow, except for the usually infuscate antennal clubs. Absolute cephalic size: 0.604 mm [0.537, 0.699]. Cephalic length vs. Maximum width of head capsule (CL/CW): 1.154 [1.116, 1.202]. Clypeal depression absent. Ground sculpture of submedian area of clypeus conspicuous areolate. Head frontal sculpture: main sculpture forked costate; rugoso-reticulate, ground sculpture conspicuous areolate; punctate. Gena sculpture: main sculpture scabrous; rugoso-reticulate, ground sculpture conspicuous areolate; punctate. Postocular distance vs. cephalic length (PoOC/CL): 0.375 [0.360, 0.389]. Eye length vs. absolute cephalic size (EL/CS): 0.224 [0.210, 0.236]. Frontal carina distance vs. absolute cephalic size (FR/CS): 0.336 [0.321, 0.358]. Scape length vs. absolute cephalic size (SL/CL): 0.804 [0.755, 0.842]. Dorsal region of mesosoma sculpture: main sculpture forked costate; rugoso-reticulate, ground sculpture conspicuous areolate; punctate. Lateral region of pronotum sculpture: main sculpture forked costate; rugoso-reticulate, ground sculpture conspicuous areolate; punctate. Mesopleuron sculpture: main sculpture forked costate; rugoso-reticulate, ground sculpture conspicuous areolate; punctate. Metapleuron sculpture: main sculpture forked costate; rugoso-reticulate, ground sculpture conspicuous areolate; punctate. Mesosoma length vs. absolute cephalic size (ML/CS): 1.198 [1.148, 1.248]. Maximum mesosoma width vs.

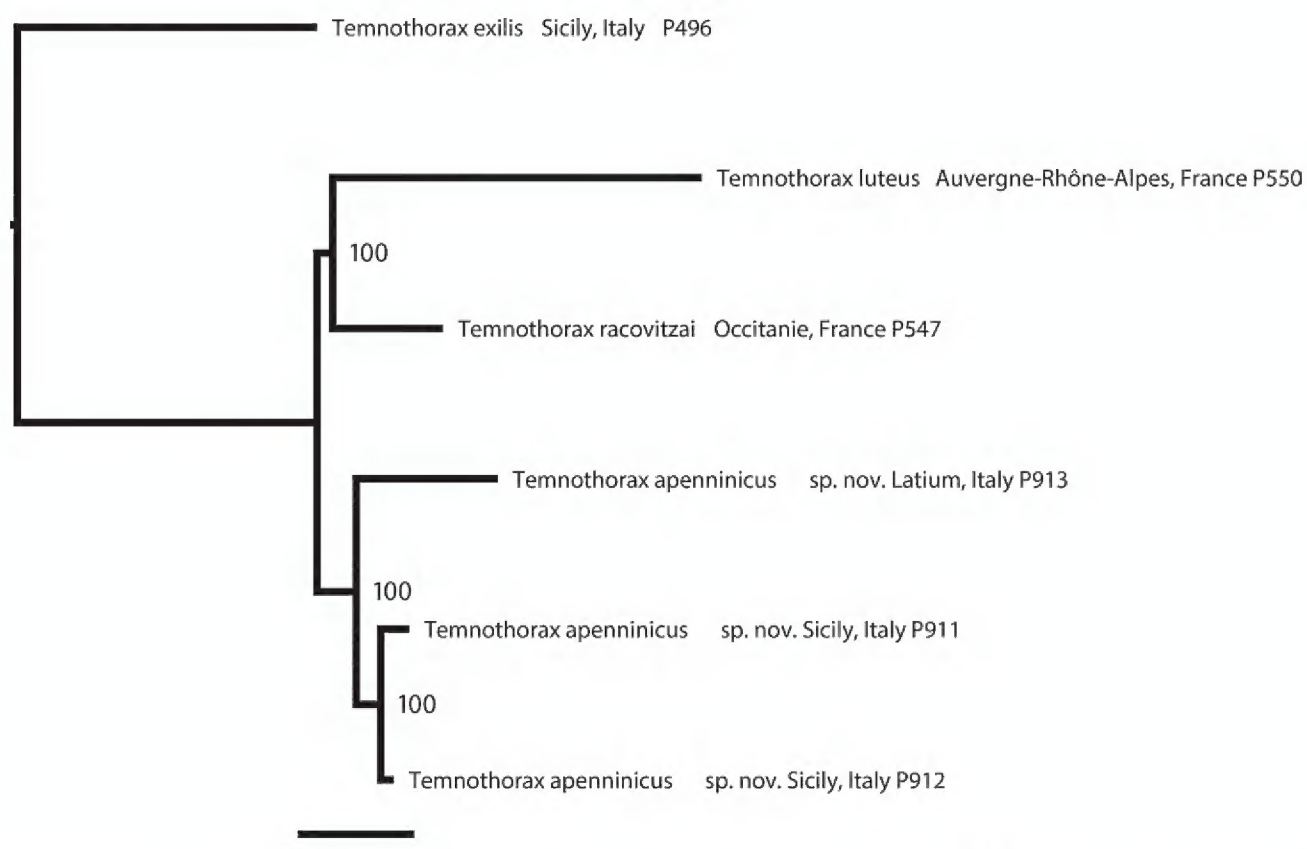
Temnothorax exilis Sicily, Italy P496
Temnothorax luteus Auvergne-Rhône-Alpes, France P550
100
Temnothorax racovitzai Occitanie, France P547
Temnothorax apenninicus sp. nov. Latium, Italy P913
100
Temnothorax apenninicus sp. nov. Sicily, Italy P911
100
Temnothorax apenninicus sp. nov. Sicily, Italy P912

Figure 4. Maximum likelihood phylogeny resulting from the partitioned analysis of 2385 ultraconserved element loci. Statistical support at each node is in bootstraps.

absolute cephalic size (MW/CS): 0.611 [0.585, 0.634]. Metanotal depression absent, the mesosomal dorsal contour line broadly convex in profile. Propodeal spines present. Propodeal spine shape: moderately long, curving downward.

Spine length vs. absolute cephalic size (SPST/CS): 0.284 [0.252, 0.320]. Minimum spine distance at its base vs. absolute cephalic size (SPBA/CS): 0.266 [0.223, 0.311]. Apical spine distance vs. absolute cephalic size (SPTI/CS): 0.341 [0.300, 0.391]. Petiole width (PEW/CS): 0.258 [0.242, 0.291]. Postpetiole width (PPW/CS): 0.349 [0.321, 0.399]. Frontal profile of petiolar node contour line in lateral view concave. Subpetiolar process well developed, tooth-like. Dorsal region of petiole sculpture: ground sculpture conspicuous areolate, main sculpture scabrous. Dorso-caudal petiolar profile contour line in lateral view broadly convex. Dorsal region of postpetiole sculpture: ground sculpture conspicuous areolate, main sculpture scabrous. Surface of the first gastral tergite smooth.

Queen (Fig. 6 A–C).

Body color yellowish brown, with anterior side of gastral tergites yellow, and appendages yellow except the infuscate antennal clubs. Head subrectangular, clypeal depression absent, clypeus smooth and shiny with vertical costae running parallel on the sides and no central carina. Head frontal sculpture: main sculpture costate in the center to areolate-rugose near the posterior and lateral margin, ground sculpture weakly areolate to smooth. Gena sculpture: main sculpture costate, ground sculpture weakly areolate. Mesosoma dorsum flat in profile view, propodeal spines well-developed, horizontal and with a wide base. Dorsal region of mesosoma sculpture: mesoscutum longitudinally costate, mesoscutellar disk largely smooth and shiny, propodeum scabrous. Lateral region of mesosoma sculpture: mostly covered in weak longitudinal costae, converging towards the spine in the propodeum, except for the katepisternum which is mostly smooth and shiny. Frontal profile of petiolar node contour line in lateral view concave. Subpetiolar process well developed,

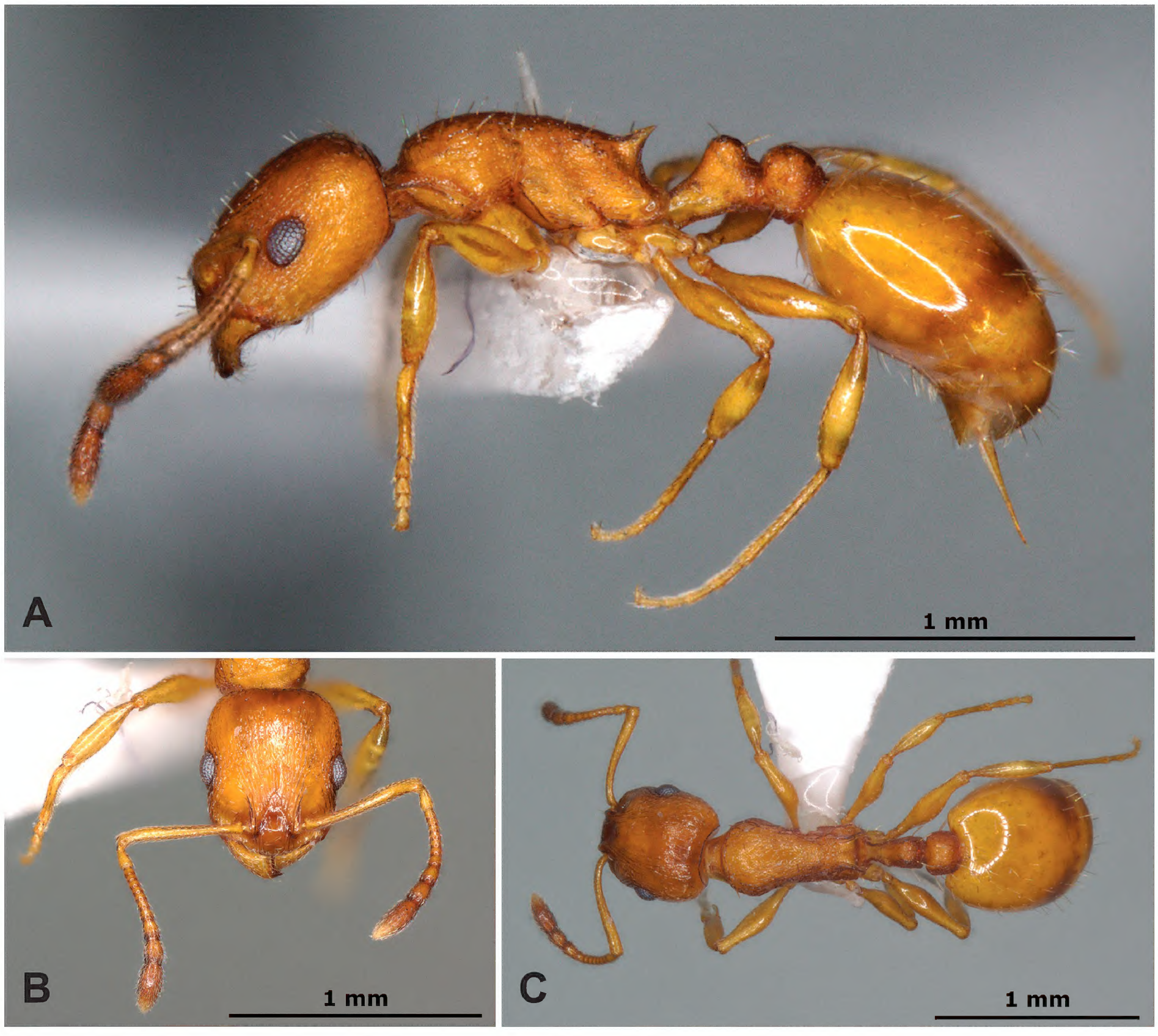

Figure 5. *Temnothorax apenninicus* worker in lateral (**A**), head (**B**), and dorsal view (**C**).

Table 3. Morphometric ratios calculated for *Temnothorax apenninicus*, *T. luteus* and *T. racovitzai* based on individuals.

	luteus (n = 104)	*racovitzai* (n = 76)	*apenninicus* (n = 40)
CS	0.624±0.048	0.586±0.032	0.604±0.034
	[0.504, 0.718]	[0.501, 0.643]	[0.537, 0.699]
CL/CW	1.134±0.022	1.133±0.017	1.154±0.023
	[1.040, 1.187]	[1.101, 1.169]	[1.116, 1.202]
POOC/	0.386±0.009	0.384±0.007	0.375±0.008
CL	[0.360, 0.410]	[0.370, 0.401]	[0.360, 0.389]
FRS/CS	0.337±0.010	0.319±0.010	0.336±0.010
	[0.318, 0.358]	[0.298, 0.339]	[0.321, 0.358]
SL/CS	0.820±0.018	0.819±0.015	0.804±0.018
	[0.760, 0.856]	[0.789, 0.849]	[0.755, 0.842]
MW/CS	0.617±0.015	0.592±0.014	0.611±0.012
	[0.578, 0.654]	[0.557, 0.630]	[0.585, 0.634]
SPBA/CS	0.272±0.017	0.255±0.015	0.266±0.018
	[0.232, 0.309]	[0.209, 0.291]	[0.223, 0.311]
SPTI/CS	0.354±0.025	0.335±0.024	0.341±0.021
	[0.304, 0.433]	[0.286, 0.406]	[0.300, 0.391]
PEW/CS	0.258±0.010	0.246±0.008	0.258±0.011
	[0.236, 0.291]	[0.229, 0.264]	[0.242, 0.291]
PPW/CS	0.346±0.013	0.337±0.012	0.349±0.017
	[0.307, 0.390]	[0.309, 0.373]	[0.321, 0.399]
ML/CS	1.216±0.023	1.163±0.020	1.198±0.021
	[1.154, 1.262]	[1.111, 1.209]	[1.148, 1.248]
SPST/CS	0.326±0.020	0.310±0.013	0.284±0.014
	[0.276, 0.372]	[0.283, 0.345]	[0.252, 0.320]
PEL/CS	0.518±0.017	0.513±0.018	0.521±0.021
	[0.469, 0.558]	[0.451, 0.563]	[0.452, 0.559]
PEH/CS	0.356±0.013	0.344±0.014	0.360±0.011
	[0.329, 0.404]	[0.320, 0.385]	[0.334, 0.388]
EYE/CS	0.216±0.006	0.224±0.006	0.224±0.006
	[0.200, 0.230]	[0.209, 0.238]	[0.210, 0.236]

tooth-like. Petiole and postpetiole sculpture: main sculpture scabrous, ground sculpture areolate. Surface of the first gastral tergite smooth.

Male (Fig. 7 A–C).

Body color brown, appendages pale yellowish. Head subtriangular, clypeal depression absent, clypeus smooth and shiny with vertical costae running parallel on the sides and no central carina. Head sculpture: ground sculpture conspicuous areolate, main sculpture carinate-rugose near the ocelli. Propodeal spines absent. Dorsal region of mesosoma sculpture: mesoscutum anteriorly smooth and posteriorly finely covered in irregurar longitudinal costae, mesoscutellar disk with fine longitudinal costae, propodeum areolate. Lateral region of mesosoma sculpture: largely areolate, katepisternum mostly smooth and shiny. Frontal profile of petiolar node contour line in lateral view concave. Petiole and postpetiole sculpture: main sculpture areolate, part of the petiolar dorsum and whole postpetiolar dorsum smooth. Surface of the first gastral tergite smooth.

Type material. ***Holotype*:** Italy, Sicily, Piano Battaglia, 37.87411, 14.02068, 1580 mH, leg. E.Schifani, 28.05.2020 (CASENT4010120, ASUHIC: Arizona State University Hasbrouck Insect Collection, Tempe, Arizona, U.S.A.).

***Paratypes*:** Altogether 37 workers are designated as paratypes, the complete list of which is also given in Suppl. material 1: Italy, Sicily, Piano Battaglia, 37.87411, 14.02068, 1580 mH, leg. E.Schifani, 28.05.2020, 3 workers; Italy, Sicily, Piano Battaglia, 37.87457, 14.01825, 1570 mH, leg. E. Schifani, 28.05.2020, 1 worker; Italy, Sicily, Monte Carbonara, 37.885949, 14.031195, 1830 mH, leg. E. Schifani, 23.05.2021, 3 workers; Italy, Sicily, Monte Carbonara, 37.886381, 14.032484, 1830 mH, leg. E. Schifani, 23.05.2021, 1 worker; Italy, Sicily, Monte Mufara, 37.874657, 14.015228, 1550 mH, leg. E. Schifani, 15.09.2022, 3 workers; Italy, Sicily, Etna Monte Scavo, 37.7733, 14.9515, 1750 mH, leg. A. Alicata, 24.07.1992, 3 workers; Italy, Sicily, Etna località Galvarina, 37.7733, 14.9513, 1850 mH, leg. A. Alicata, 22.07.1992, 3 workers; Italy, Sicily, Etna Monte Maletto, 37.7733, 14.9513, 1850 mH, leg. A. Alicata, 22.07.1992, 3 workers; Italy, Sicily, Etna Monte Maletto, 1850 mH, leg. A. Alicata, 22.07.1992, 3 workers; Italy, Sicily, Etna Monte Ruvolo, 37.7480, 14.8910, 1400 mH, leg. A. Alicata, 18.08.1992, 3 workers; Italy, Sicily, Etna Monte Sona, 37.66688, 14.9843, 1390 mH, leg. A. Alicata, 16.05.1992, 3 workers; Italy, Sicily, Etna Monte S. Maria, 37.8240, 14.990, 1632 mH, leg. A. Alicata, 05.09.1992, 2 workers; Italy, Sicily, Etna, 2000 mH, leg. A. Alicata, 10.07.1993, 3 workers; Italy, Calabria, Pollino National Park – Pian Grande, 39.833595, 16.053456, 1230 mH, leg. A. Alicata, 27.08.2021, 3 workers; Italy, Latium, Pratone di Monte Gennaro, 42.05880, 12.82697, 1020 mH, leg. V. Dolci, 03.09.2017, 2 workers; Italy, Lombardy, Riserva Naturale Boschi del Giovetto di Palline, 45.955014 10.125193, 1462 mH, leg. E. Schifani, 25.06.2019, 2 workers; The paratypes are deposited in the following institutions: HNHM (Hungarian Natural History Museum, Budapest, Hungary), MHNG (Muséum d'histoire naturelle, Genf, Switzerland), NHMB (Naturhistorisches Museum Basel, Switzerland), NHMW (Naturhistorisches Museum Wien, Austria), SCPC (Private collection of SC), SMNG (Senckenberg Museum für Naturkunde Görlitz, Germany).

Etymology. The name refers to the Apennines Mountains that span from Sicily to northern Italy, encompassing most of the species' distribution and likely constituting its glacial refugium.

Morphological diagnosis. The only qualitative difference between *T. apenninicus* and *T. luteus* is represented by the normally infuscate antennal clubs and infuscate first gastral tergite of the first (features that may be subsequently lost depending on the preservation state of the specimens). In the Italian fauna, a chromatic pattern superficially similar to *T. apenninicus* is known for *T. minozzii* (Santschi 1922), which is however characterized by much shorter spines, a different petiole shape and a smooth head sculpture, and only known from a lowland site.

The three species considered in this revision represent otherwise true cryptic species, as no single morphometric ratio allows for separation at the individual level. The nest sample mean values spine length ratio (SPST/CS) help to tell *Temnothorax apenninicus* sp. nov. workers apart from its congeners *T. luteus* and *T. racovitzai* with an acceptably high success rate (Fig. 8, Table 4). However, a narrow overlap is still present.

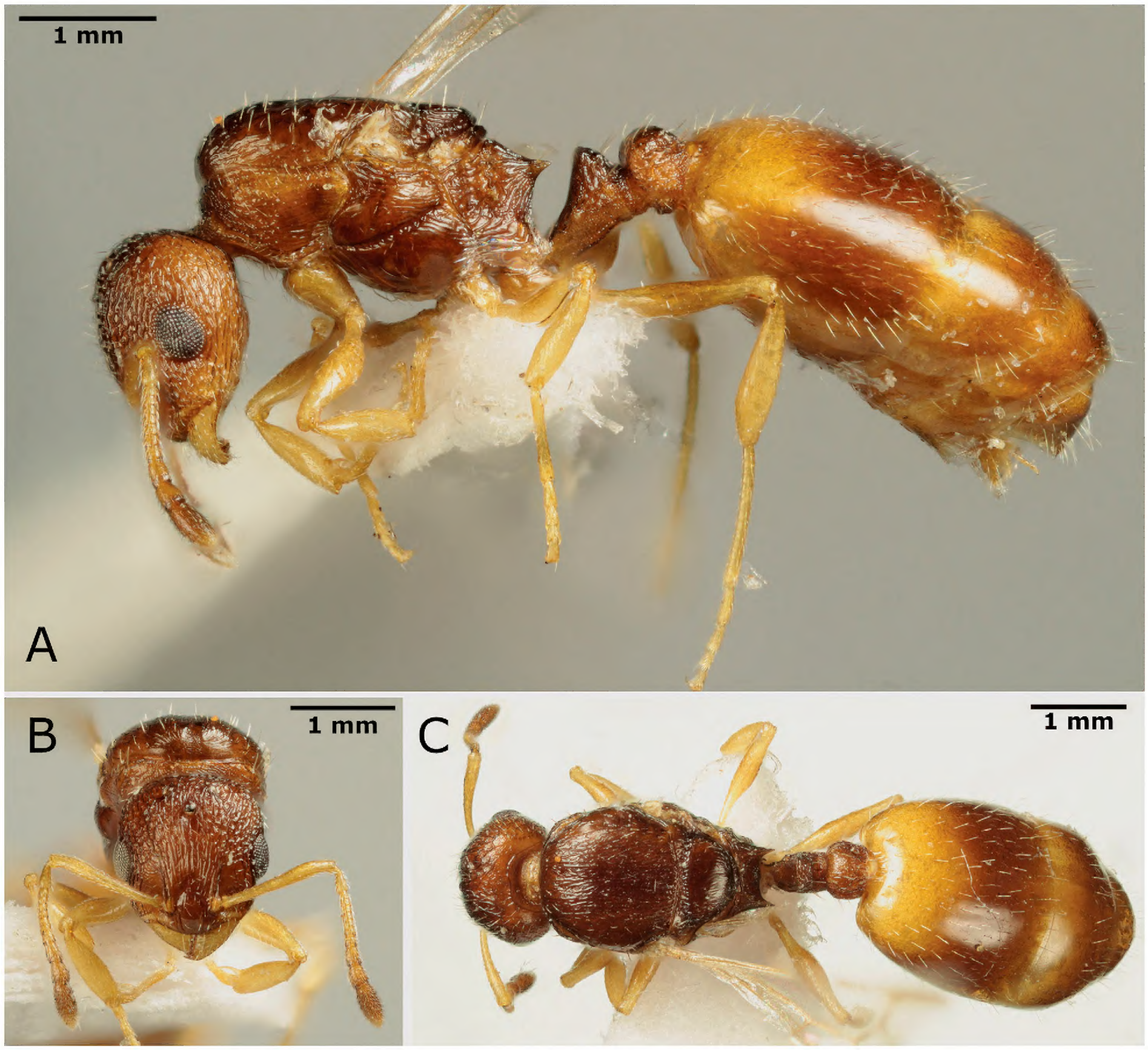

Figure 6. *Temnothorax apenninicus* queen in lateral (**A**), head (**B**), and dorsal view (**C**).

The striking morphological similarity does not allow drastic trait reduction in individual workers while maintaining the desired classification success in the three-species scenarios. However, if species pairs are considered, *T. apenninicus* can be easily separated from *T. luteus* and *T. racovitzai* based on a combination of three morphometric traits.

Between *T. apenninicus* and *T. luteus*, the combination of three traits D3a = 79.6279 *CL -117.9626 *POO -94.5116 *SPST -5.015 yields only five misclassified cases out of the total 145 individuals, with an overall accuracy of 0.966, [95% CI: (0.921, 0.989)] or permitting 3.4% error rate (Fig. 9).

Discriminant (D3a) scores for the species are as follows:

D3a apenninicus (n = 40) = +1.71 [-0.67, +3.74]
D3a luteus (n = 104) = -1.71 [-4.46, +1.89]

Separating *T. apenninicus* from *T. racovitzai* can be safely achieved based on the following traits: D3b = 72.92828*ML -68.1532*SL -95.02586*SPST -1.566. This function yields only four misclassified cases out of the total 118 individuals, with an overall accuracy of 0.966, [95% CI: (0.914, 0.991)] or permitting a 3.4% error rate (Fig. 10).

Discriminant (D3b) scores for the species are as follows:

D3b apenninicus (n = 40) = +1.819 [-0.191, +4.096]
D3b racovitzai (n = 78) = -1.819 [-4.764, +0.787]

Distribution and ecology. The range extends from Sicily to the Alps (Fig. 11). *Temnothorax apenninicus* appears to be a mountain species that lives preferably in meadows and open habitats. Nests are built opportunistically on the ground, in rock crevices, or under stones. Most of our data come from the southern portion of *T. apenninicus* distribution range: *T. apenninicus* is probably the highest elevation *Temnothorax* species in Sicily (Etna, Mt. Carbonara), ranging from 1400 to 2000 m. At higher latitudes, we expect a downshift of the elevational range, with the single record from central Italy (Latium) at 1020 m, and the one from the southern edge of the Alps at 1460 m. On the Etna, multiple colonies were found to be parasitized by the social parasite *T. muellerianus*

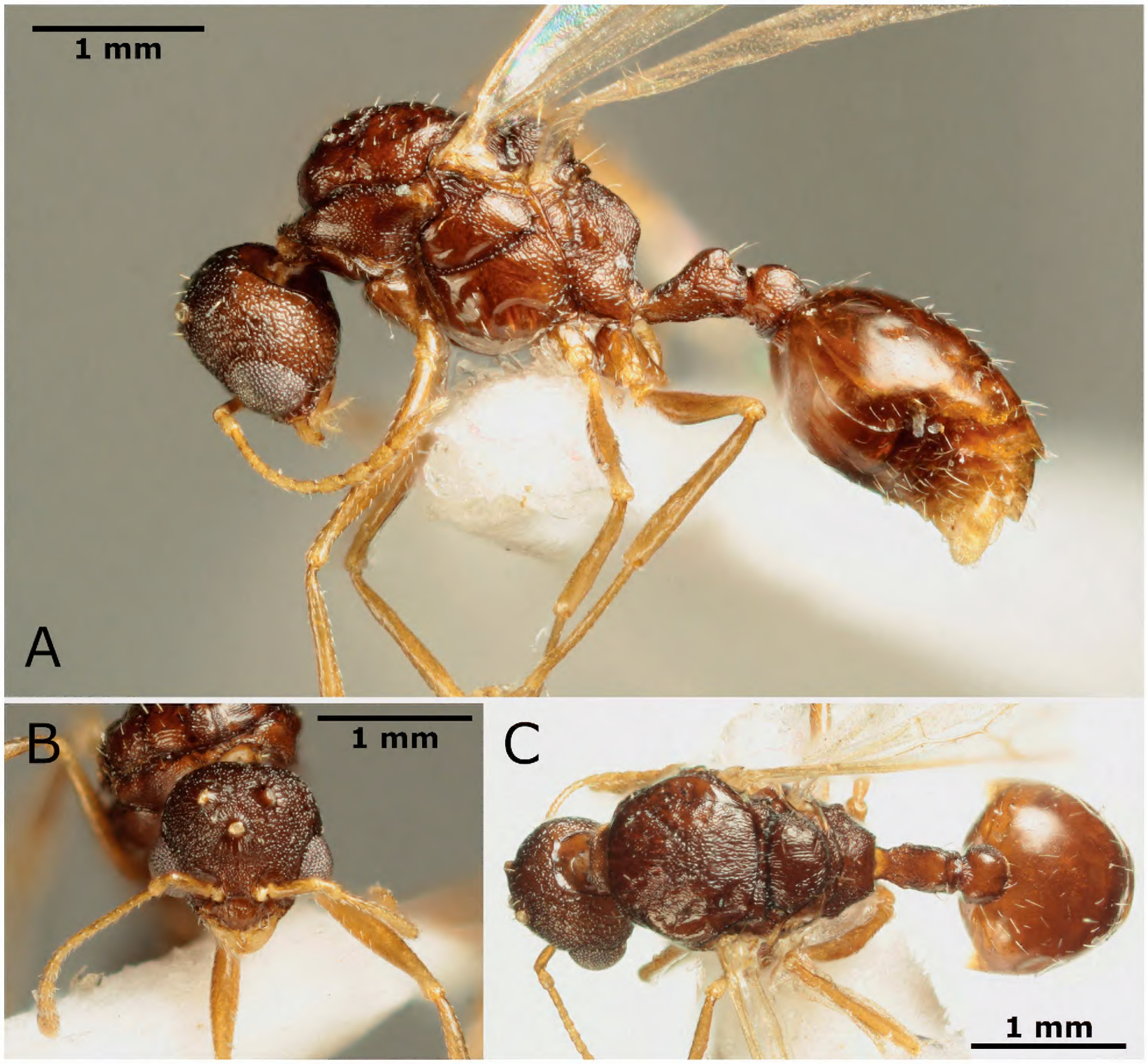

Figure 7. *Temnothorax apenninicus* male in lateral (**A**), head (**B**), and dorsal view (**C**).

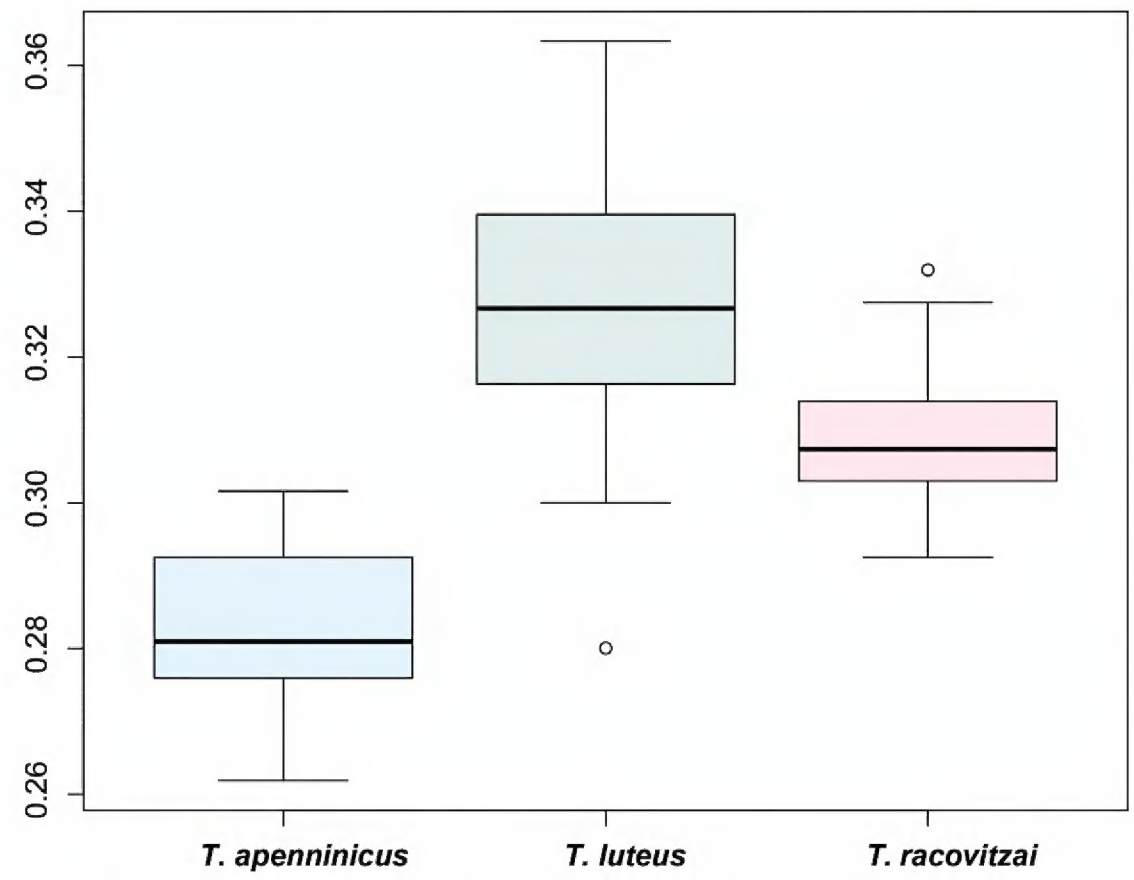

Figure 8. Quartiles that partition spine length ratio nest sample mean values (SPST/CS). Lower and upper extremes, and 25%, 50%, 75% quantiles are shown.

Table 4. Quartiles that partition spine length ratio nest sample mean values (SPST/CS). Lower and upper extremes, and 25%, 50%, 75% quantiles are shown.

Quartiles:	Lower	25%	50%	75%	Upper
T. apenninicus	0.262	0.276	0.281	0.292	0.302
T. luteus	0.280	0.316	0.327	0.339	0.363
T. racovitzai	0.293	0.303	0.307	0.314	0.332

(Finzi, 1922) also referred to as *Chalepoxenus muellerianus* (see Ward et al. 2015, 2016; Seifert et al. 2016). Buschinger et al. (1988) noted that the local population of this social parasite (previously known as *Chalepoxenus siciliensis* Kutter, 1973) seemed to have specialized in parasitizing a species "close to *Leptothorax tristis*" (i.e., a former name of *T. luteus*), which most likely was *T. apenninicus*.

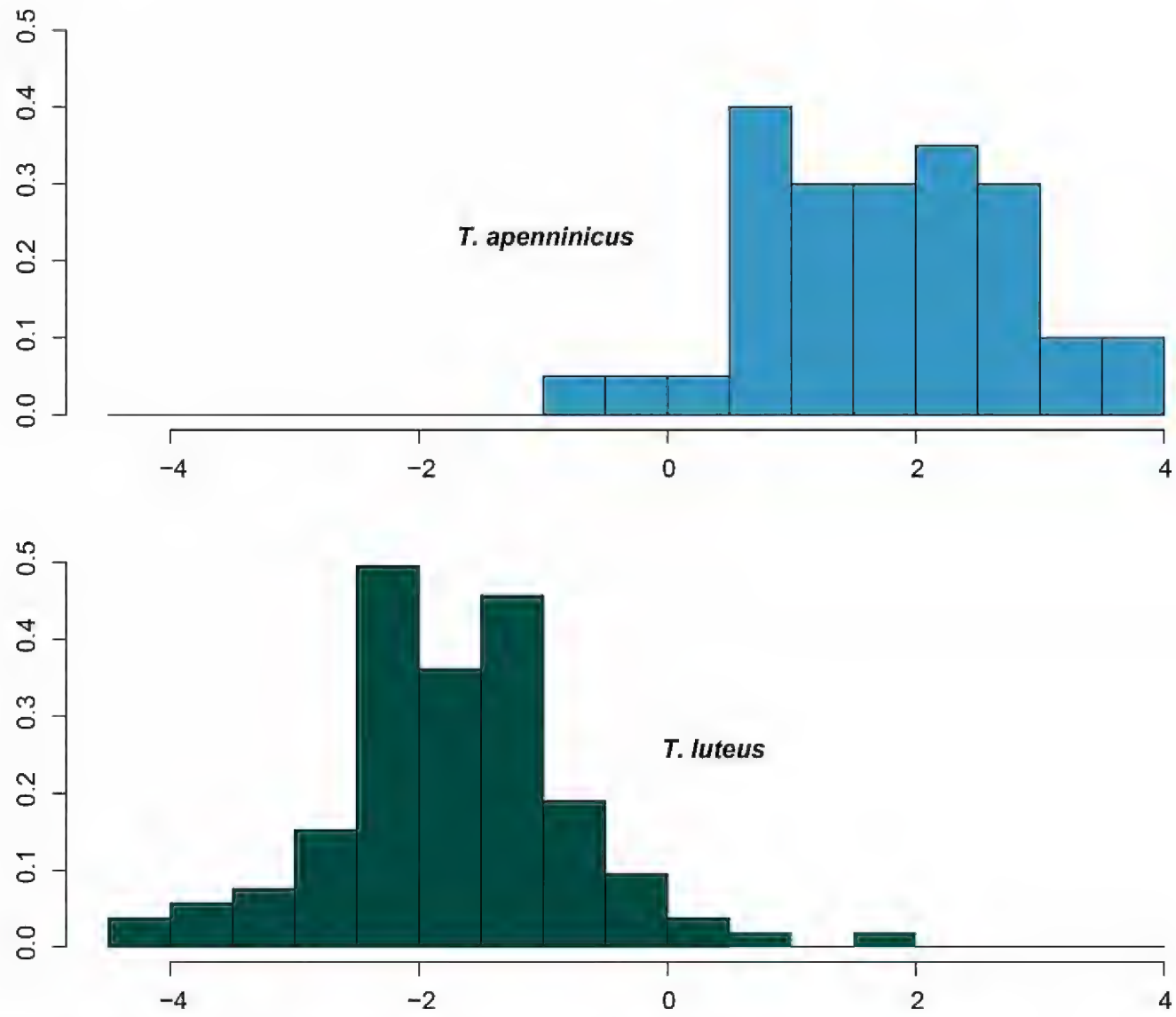

Figure 9. Discriminant (D3a) scores for *Temnothorax apenninicus* and *T. luteus* worker individuals.

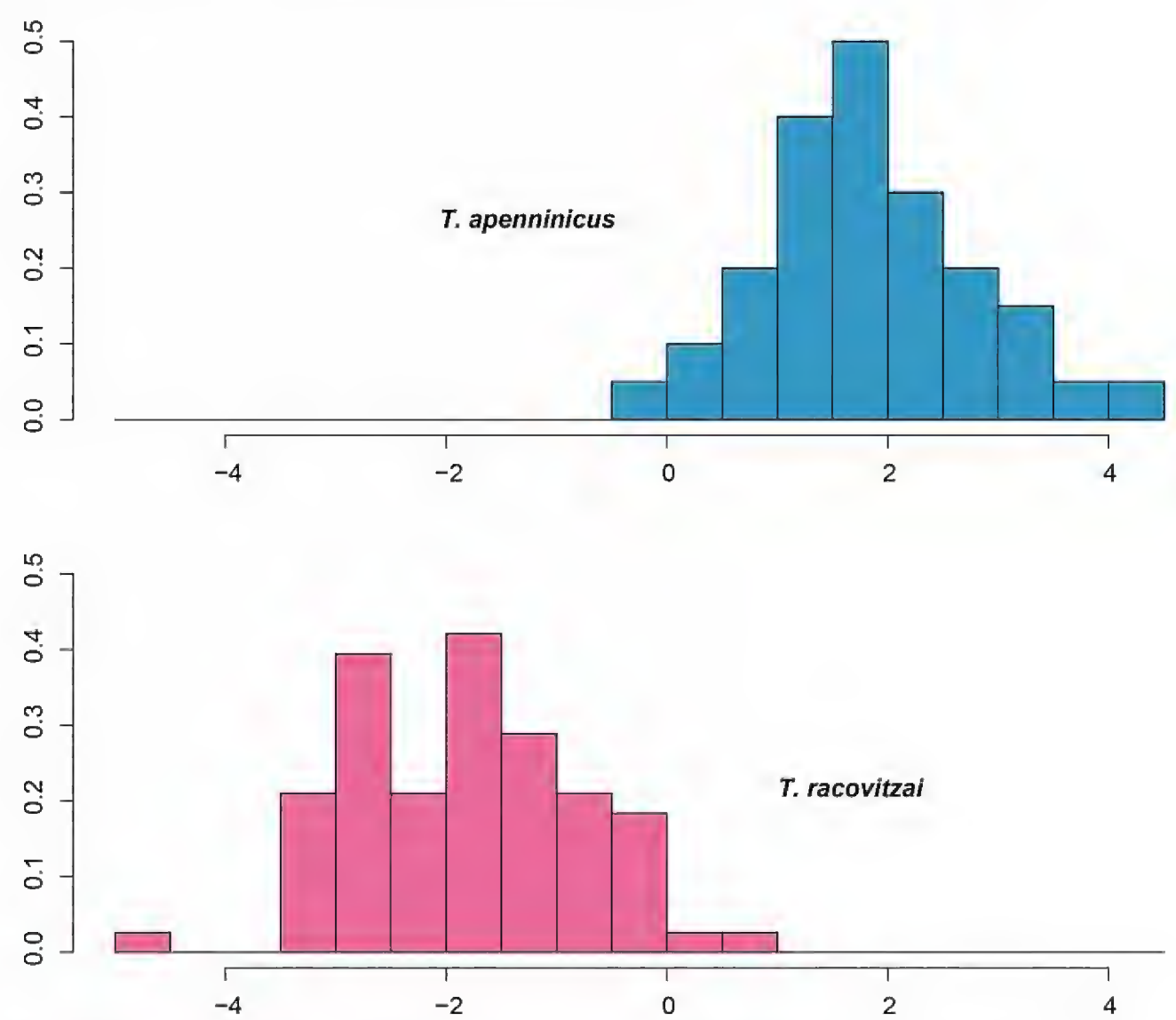

Figure 10. Discriminant (D3b) scores for *Temnothorax apenninicus* and *T. racovitzai* worker individuals.

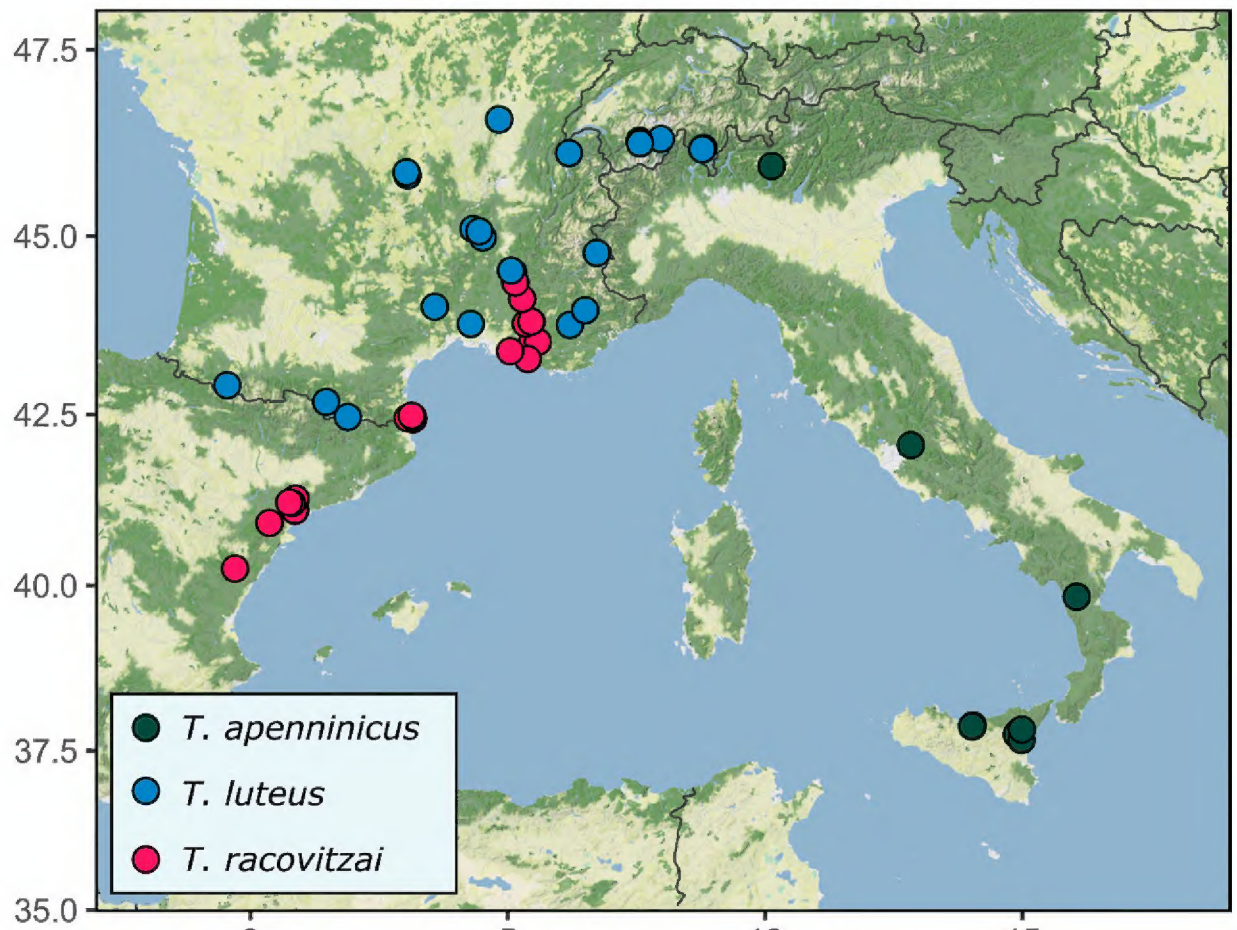

Figure 11. Distribution map of the *Temnothorax* samples analyzed in this study. Map from Stadia Maps - stadiamaps.com and Stamen Design (stamen.com), plotted using the R package "ggmap" (Kahle and Wickham 2013).

Dichotomic key for worker specimens' identification

The W-European representatives of the *T. luteus* complex represent a morphologically cryptic triad, hence only a combination of morphometric traits can yield safe solutions in separating these species.

1 In the nest sample mean (3 workers or more), the spine length ratio (SPST/CS) lower than 0.3. For singletons, use Discriminant D3a and D3b (Figs 9, 10) ..... *T. apenninicus* sp. nov.
– In the nest sample mean (3 workers or more), the spine length ratio (SPST/CS) higher than 0.3 (see Fig. 8). For singletons, use Discriminant D3a and D3b (Figs 9, 10) 2
2 In the nest sample mean, Discriminant D4a 74.496*FRS–206.142*EYE+57.695*ML –49.634*CL+2.636 = –1.996 ± 0.74 [–3.113, –0.435] with no interspecific overlap. Values for singletons are –2.044 ± 0.88 [–4.363, 0.041], with a 3.9% error rate recorded (Seifert et al. 2014) ..... *T. racovitzai*
– In the nest sample mean, D4a values 1.380 ± 0.83 [–0.157, 3.779]. Values for singletons are 1.388 ± 1.07 [–1.051, 4.433] ..... *T. luteus*

Discussion

The discovery of *T. apenninicus*, stretching from Sicily to the Italian Alps, is paired with the absence of *T. luteus* and *T. racovitzai* records in the same range. The easternmost distribution of *T. luteus* reaches the French and Swiss Alps, and the species is likely present on the western side of the Italian Alps as well (Menchetti et al. unpublished data), so the contact range of the two certainly requires further investigation. However, the few and scattered previous *T. luteus* records in Italy were most likely based on misidentifications of *T. apenninicus* if not of other taxa (Baroni Urbani 1971; Schifani et al. 2022, 2024).

Our results reinforce the previous hypothesis that *T. racovitzai* may have colonized France from an Iberian glacial refugium (Seifert et al. 2014), as it does not appear to occur east of France. While the southern Apennines must have been the glacial refugium of *T. apenninicus*, *T. luteus* may have been perhaps isolated in the western Alps (Taberlet et al. 1998; Menchetti et al. 2021; Schmitt et al. 2021). While some morphologically more distinct species may belong to the *luteus* group *sensu lato* both on the western (e.g., *T. pardoi* (Tinaut, 1987), see Gouraud et al. 2021) or perhaps even eastern Mediterranean basin (e.g., as suggested for the Cretan *T. variabilis* Salata, Borowiec & Trichas, 2018 – see Salata et al. 2018), no phylogenetic data are yet available to assess this hypothesis and the definition of *Temnothorax* species groups solely based on qualitative morphological characters remains elusive (Schifani et al. 2022).

Italy hosts several endemic ant species, with no assessment of their conservation status available yet (Schifani 2022). Only very few of these, including *T. apenninicus*, seem to be restricted to high elevations – including one, *Aphaenogaster italica* with a distribution very similar to *T. apenninicus* (Radchenko et al. 2006; Schifani and Alicata 2018). The status of these species should receive attention considering the threat climate change is posing to mountain ecosystems (Guisan et al. 2019; Schifani et al. 2024).

While molecular evidence is expanding our understanding of intrageneric relationships in *Temnothorax* (Prebus 2017), the picture in the Mediterranean is still very incomplete on many fronts, and not all groups are easily delimited on a morphological basis (Schifani et al. 2022). Further investigations will be helpful to identify other potential relatives of the *T. luteus* complex in neighboring regions, such as Iberia and the Maghreb, and eventually attain a clearer picture of the diversity of the whole *rottenbergii* clade (Prebus 2017).

Acknowledgments

We thank Valerio Dolci (Italy) and Christophe Galkowski (France) for handling us some samples used in this study. This project has received funding from the HUN-REN Hungarian Research Network. This research was co-financed by the National Research, Development, and innovation Fund (Hungary) under Grant No. K 147781 (On behalf of SC). MMP was supported by the US National Science Foundation (NSF CAREER DEB-1943626), the Social Insect Research Group (SIRG) at Arizona State University, the University of Hohenheim, and the Carl-Zeiss-Foundation. The equipment for digital imaging was co-financed by tax money on the basis of the state budget passed by the Sächsischer Landtag according to the Antragsnummer 100590787 of the Sächsische Aufbaubank issued 3 August 2021.

References

Arcos J, García F (2023) Hormigas de la península Ibérica e islas Baleares. Independently published, Spain, 491 pp.

Baroni Urbani C (1971) Catalogo delle specie di Formicidae d'Italia. Memorie della Società Entomologica Italiana 50: 5–287.

Bolton B (2024) An Online Catalog of the Ants of the World. https://antcat.org [accessed 10 Mar. 2024]

Branstetter MG, Longino JT, Ward PS, & Faircloth BC (2017) Enriching the ant tree of life: enhanced UCE bait set for genome-scale phylogenetics of ants and other Hymenoptera. Methods in Ecology and Evolution 8(6): 768–776. https://doi.org/10.1111/2041-210X.12742

Buckley TR, Simon C, Chambers GK (2001) Exploring among-site rate variation models in a maximum likelihood framework using empirical data: effects of model assumptions on estimates of topology, branch lengths, and bootstrap support. Systematic Biology 50(1): 67–86. https://doi.org/10.1080/10635150116786

Castresana J (2000) Selection of conserved blocks from multiple alignments for their use in phylogenetic analysis. Molecular Biology and Evolution 17(4): 540–552. https://doi.org/10.1093/oxfordjournals.molbev.a026334

Csősz S, Fisher BL (2016) Taxonomic revision of the Malagasy members of the *Nesomyrmex angulatus* species group using the automated morphological species delineation protocol NC-PART-clustering. PeerJ 4: e1796. https://doi.org/10.7717/peerj.1796

Csősz S, Seifert B, Mikó I, Boudinot BE, Borowiec ML, Fisher BL, Prebus M, Puniamoorthy J, Rakotonirina J-C, Rasoamanana N, Schultz R, Trietsch C, Ulmer JM, Elek Z (2021) Insect morphometry is reproducible under average investigation standards. Ecology and evolution 11(1): 547–559. https://doi.org/10.1002/ece3.7075

Faircloth BC (2016) PHYLUCE is a software package for the analysis of conserved genomic loci. Bioinformatics 32(5): 786–788. https://doi.org/10.1093/bioinformatics/btv646

Faircloth BC, Branstetter MG, White ND, Brady SG (2015) Target enrichment of ultraconserved elements from arthropods provides a genomic perspective on relationships among Hymenoptera. Molecular Ecology Resources 15(3): 489–501. https://doi.org/10.1111/1755-0998.12328

Giannetti D, Schifani E, Castracani C, Mori A, Grasso DA (2022a) The introduced oak *Quercus rubra* and acorn-associated arthropods in Europe: an opportunity for both carpophagous insects and their ant predators. Ecological Entomology 47(4): 515–526. https://doi.org/10.1111/een.13136

Giannetti D, Schifani E, Castracani C, Spotti FA, Mori A, Grasso DA (2022b) Different nest entrance architecture by *Colobopsis* and *Temnothorax* ants colonizing oak galls. Insectes Sociaux 69: 383–388. https://doi.org/10.1007/s00040-022-00884-2

Giannetti D, Schifani E, Gugliuzzo A, Zappalà L, Biondi A, Grasso DA (2022c) Native European ants can discourage host colonization and reduce reproductive success of the invasive ambrosia beetle *Xylosandrus compactus*. Biological Control 174: 105032. https://doi.org/10.1016/j.biocontrol.2022.105032

Glenn TC, Nilsen RA, Kieran TJ, Sanders JG, Bayona-Vásquez NJ, Finger JW, Pierson TW, Bentley KE, Hoffberg SL, Louha S, Garcia-De Leon FJ, del Rio Portilla MA, Reed KD, Anderson JL, Meece JK, Aggrey SE, Rekaya R, Alabady M, Belanger M, Winker K, Faircloth BC (2019) Adapterama I: universal stubs and primers for 384 unique dual-indexed or 147,456 combinatorially-indexed Illumina libraries (iTru & iNext). PeerJ 7: e7755. https://doi.org/10.7717/peerj.7755

Gouraud C, Raitière C, Galkowski C (2021) *Temnothorax pardoi* (Tinaut, 1987) en Bretagne, une espèce sténotope inféodée aux landes? Invertébrés Armoricains 22: 11–20.

Guisan A, Broennimann O, Buri A, Cianfrani C, D'Amen M, Di Cola V, Fernandes R, Gray SM, Mateo RG, Pinto E, Pradervand J-N, Scherrer D, Vittoz P, Von Däniken I, Yashiro E (2019) Climate change impacts on mountain biodiversity. Biodiversity and Climate Change 221–233. https://doi.org/10.12987/9780300241198-026

Kahle D, Wickham H (2013) ggmap: Spatial Visualization with ggplot2. The R Journal 5: 1. https://doi.org/10.32614/rj-2013-014

Kass JM, Guénard B, Dudley KL, Jenkins CN, Azuma F, Fisher BL, Parr CL, Gibb H, Longino JT, Ward PS, Chao A, Lubertazzi D, Weiser M, Jetz W, Guralnick R, Blatrix R, Des Lauriers J, Donoso DA, Georgiadis C, Gomez K, Hawkes PG, Johnson RA, Lattke JE, MacGown JA, Mackay W, Robson S, Sanders NJ, Dunn RR, Economo EP (2022) The global distribution of known and undiscovered ant biodiversity. Science advances 8(31): eabp9908. https://doi.org/10.1126/sciadv.abp9908

Katoh K, Standley DM (2013) MAFFT multiple sequence alignment software version 7: improvements in performance and usability. Molecular Biology and Evolution 30(4): 772–780. https://doi.org/10.1093/molbev/mst010

Menchetti M, Talavera G, Cini A, Salvati V, Dincă V, Platania L, Bonelli S, Balletto E, Vila R, Dapporto L (2021) Two ways to be endemic. Alps and Apennines are different functional refugia during climatic cycles. Molecular Ecology 30(5): 1297–1310. https://doi.org/10.1111/mec.15795

Nilsen G, Lingjaerde OC (2013) clusterGenomics: Identifying clusters in genomics data by recursive partitioning. R package

version 1.0. [retrived on 10 January 2017] https://doi.org/10.1515/sagmb-2013-0016

Prebus M (2015) Palearctic elements in the old world tropics: a taxonomic revision of the ant genus *Temnothorax* Mayr (Hymenoptera, Formicidae) for the Afrotropical biogeographical region. Zookeys 483: 23. https://doi.org/10.3897/zookeys.483.9111

Prebus M (2017) Insights into the evolution, biogeography and natural history of the acorn ants, genus *Temnothorax* Mayr (hymenoptera: Formicidae). BMC Evolutionary Biology 17: 250. https://doi.org/10.1186/s12862-017-1095-8

R Core Team (2022) R: A language and environment for statistical computing. R Foundation for Statistical Computing, Vienna, Austria. https://www.R-project.org/

Radchenko A, Elmes GW, Alicata A (2006) Taxonomic revision of the schencki-group of the ant genus Myrmica Latreille (Hymenoptera: Formicidae) from the Palaearctic region. Annales Zoologici 56(3): 499–538.

Rohland N, Reich D (2012) Cost-effective, high-throughput DNA sequencing libraries for multiplexed target capture. Genome Research 22(5): 939–946. https://doi.org/10.1101/gr.128124.111

Salata S, Borowiec L, Trichas A (2018) Taxonomic revision of the Cretan fauna of the genus *Temnothorax* Mayr, 1861 (Hymenoptera: Formicidae), with notes on the endemism of ant fauna of crete. Annales Zoologici 68: 769–808. https://doi.org/10.3161/00034541ANZ2018.68.4.004

Schifani E (2022) The new Checklist of the Italian Fauna: Formicidae. Biogeographia 37: ucl006. https://doi.org/10.21426/B637155803

Schifani E, Alicata A (2018) Exploring the myrmecofauna of Sicily: thirty-two new ant species recorded, including six new to Italy and many new aliens (Hymenoptera, Formicidae). Polish Journal of Entomology 87(4): 323–348. https://doi.org/10.2478/pjen-2018-0023

Schifani E, Prebus MM, Alicata A (2022) Integrating morphology with phylogenomics to describe four island endemic species of *Temnothorax* from Sicily and Malta (Hymenoptera, Formicidae) European Journal of Taxonomy 833: 143–179. https://doi.org/10.5852/ejt.2022.833.1891

Schifani E, Grasso DA, Gobbi M, Spotti FA, Pedrotti L, Vettorazzo E, Mori A, Castracani C (2024) Ant diversity along elevational gradients in the European Alps: insights for conservation under a changing climate. Journal of Insect Conservation. https://doi.org/10.1007/s10841-023-00546-z

Schlick-Steiner BC, Steiner FM, Seifert B, Stauffer C, Christian E, Crozier RH (2010) Integrative taxonomy: a multisource approach to exploring biodiversity. Annual review of entomology 55: 421–438. https://doi.org/10.1146/annurev-ento-112408-085432

Schmitt T, Fritz U, Delfino M, Ulrich W, Habel JC (2021) Biogeography of Italy revisited: genetic lineages confirm major phylogeographic patterns and a pre-Pleistocene origin of its biota. Frontiers in Zoology 18: 1–13. https://doi.org/10.1186/s12983-021-00418-9

Seifert B (2018) The Ants of Central and North Europe. Lutra Verlags-und Vertriebsgesellschaft, Tauer, Germany, 408 pp.

Seifert B, Csősz S, Schulz A (2014) NC-Clustering demonstrates heterospecificity of the cryptic ant species *Temnothorax luteus* (Forel, 1874) and *T. racovitzai* (Bondroit, 1918) (Hymenoptera: Formicidae). Beiträge zur Entomologie 64(1): 47–57. https://doi.org/10.21248/contrib.entomol.64.1.47-57

Seifert B, Buschinger A, Aldawood A, Antonova V, Bharti H, Borowiec L, Dekoninck W, Dubovikoff D, Espadaler X, Flegr J, Georgiadis C, Heinze J, Neumeyer R, Ødegaard F, Oettler J, Radchenko A, Schultz R, Sharaf M, Trager J, Vesnić A, Wiezik M, Zettel H (2016) Banning paraphylies and executing Linnaean taxonomy is discordant and reduces the evolutionary and semantic information content of biological nomenclature. Insectes Sociaux 63: 237–242. https://doi.org/10.1007/s00040-016-0467-1

Sullivan J, Swofford DL (2001) Should we use model-based methods for phylogenetic inference when we know that assumptions about among-site rate variation and nucleotide substitution pattern are violated? Systematic Biology 50(5): 723–729. https://doi.org/10.1080/106351501753328848

Taberlet P, Fumagalli L, Wust-Saucy AG, Cosson JF (1998) Comparative phylogeography and postglacial colonization routes in Europe. Molecular Ecology 7(4): 453–464. https://doi.org/10.1046/j.1365-294x.1998.00289.x

Tagliacollo VA, Lanfear R (2018) Estimating improved partitioning schemes for ultraconserved elements. Molecular Biology and Evolution 35(7): 1798–1811. https://doi.org/10.1093/molbev/msy069

Venables WN, Ripley BD (2002) Modern Applied Statistics with S, Fourth edition. Springer, New York. [ISBN 0-387-95457-0] https://www.stats.ox.ac.uk/pub/MASS4/

Wang R, Kass JM, Galkowski C, Garcia F, Hamer MT, Radchenko A, Salata S, Schifani E, Yusupov ZM, Economo EP, Guénard B (2023) Geographic and climatic constraints on bioregionalization of European ants. Journal of Biogeography 50: 503–514. https://doi.org/10.1111/jbi.14546

Ward PS, Brady SG, Fisher BL, Schultz TR (2015) The evolution of myrmicine ants: Phylogeny and biogeography of a hyperdiverse ant clade (Hymenoptera: Formicidae). Systematic Entomology 40: 61–81. https://doi.org/10.1111/syen.12090

Ward PS, Brady SG, Fisher BL, Schultz TR (2016) Phylogenetic classifications are informative, stable, and pragmatic: the case for monophyletic taxa. Insectes Sociaux 63: 489–492. https://doi.org/10.1007/s00040-016-0516-9

Wolak ME, Fairbairn DJ, Paulsen YR (2012) Guidelines for estimating repeatability. Methods in Ecology and Evolution 3: 129–137. https://doi.org/10.1111/j.2041-210X.2011.00125.x

Yang Z (2006) Computational molecular evolution. OUP Oxford, New York, 353 pp. https://doi.org/10.1093/acprof:oso/9780198567028.001.0001

Supplementary material 1

Material examined in this study

Authors: Sándor Csősz, Bernhard Seifert
Data type: xlsx
Explanation note: The complete list of examined material, including locality information, number of measured individuals is enlisted.
Copyright notice: This dataset is made available under the Open Database License (http://opendatacommons.org/licenses/odbl/1.0). The Open Database License (ODbL) is a license agreement intended to allow users to freely share, modify, and use this Dataset while maintaining this same freedom for others, provided that the original source and author(s) are credited.
Link: https://doi.org/10.3897/evolsyst.8.124557.suppl1

Supplementary material 2

Morphometric data of worker individuals

Authors: Sándor Csősz, Bernhard Seifert
Data type: xlsx
Explanation note: Raw data are given in millimeters.
Copyright notice: This dataset is made available under the Open Database License (http://opendatacommons.org/licenses/odbl/1.0). The Open Database License (ODbL) is a license agreement intended to allow users to freely share, modify, and use this Dataset while maintaining this same freedom for others, provided that the original source and author(s) are credited.
Link: https://doi.org/10.3897/evolsyst.8.124557.suppl2

Supplementary material 3

Collection data for sequenced samples

Authors: Enrico Schifani, Matthew M. Prebus
Data type: xlsx
Copyright notice: This dataset is made available under the Open Database License (http://opendatacommons.org/licenses/odbl/1.0). The Open Database License (ODbL) is a license agreement intended to allow users to freely share, modify, and use this Dataset while maintaining this same freedom for others, provided that the original source and author(s) are credited.
Link: https://doi.org/10.3897/evolsyst.8.124557.suppl3

Supplementary material 4

Summary statistics for molecular phylogeny

Author: Matthew M. Prebus
Data type: xlsx
Copyright notice: This dataset is made available under the Open Database License (http://opendatacommons.org/licenses/odbl/1.0). The Open Database License (ODbL) is a license agreement intended to allow users to freely share, modify, and use this Dataset while maintaining this same freedom for others, provided that the original source and author(s) are credited.
Link: https://doi.org/10.3897/evolsyst.8.124557.suppl4